

# Journal of Materials Chemistry C

Accepted Manuscript



This is an *Accepted Manuscript*, which has been through the Royal Society of Chemistry peer review process and has been accepted for publication.

*Accepted Manuscripts* are published online shortly after acceptance, before technical editing, formatting and proof reading. Using this free service, authors can make their results available to the community, in citable form, before we publish the edited article. We will replace this *Accepted Manuscript* with the edited and formatted *Advance Article* as soon as it is available.

You can find more information about *Accepted Manuscripts* in the [Information for Authors](#).

Please note that technical editing may introduce minor changes to the text and/or graphics, which may alter content. The journal's standard [Terms & Conditions](#) and the [Ethical guidelines](#) still apply. In no event shall the Royal Society of Chemistry be held responsible for any errors or omissions in this *Accepted Manuscript* or any consequences arising from the use of any information it contains.

## 9,9'-Spirobifluorene and 4-Phenyl-9,9'-Spirobifluorene: Pure Hydrocarbon Small Molecules as Hosts for efficient Green and Blue PhOLEDs

Sébastien Thiery,<sup>†</sup> Denis Tondelier,<sup>§</sup> Céline Declairieux,<sup>§</sup> Gijun Seo,<sup>§</sup> Bernard Geffroy,<sup>§</sup> Olivier Jeanin,<sup>†</sup> Joëlle Rault-Berthelot,<sup>†\*</sup> Rémi Métivier,<sup>‡</sup> Cyril Poriel<sup>†\*</sup>

<sup>†</sup> Université de Rennes 1-UMR CNRS 6226 "Sciences Chimiques de Rennes"- MaCSE group, Bat 10C, Campus de Beaulieu-35042 Rennes cedex, France

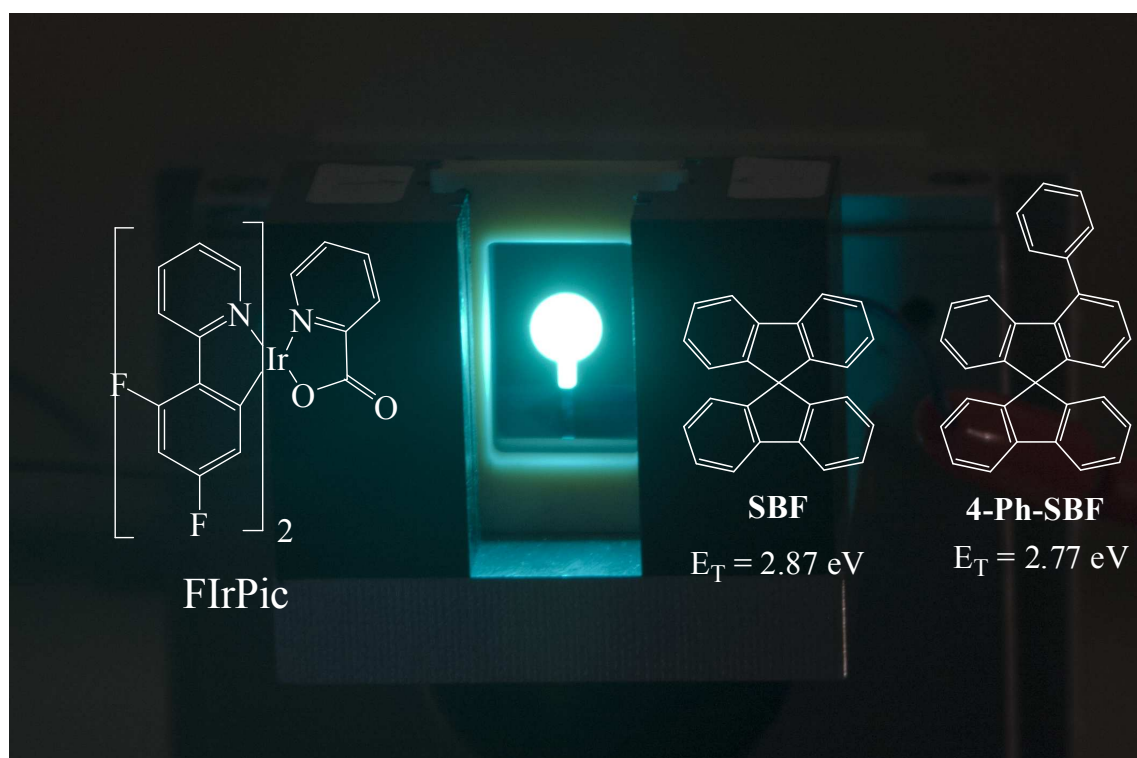
<sup>‡</sup> PPSM ENS Cachan, UMR CNRS 8531, 61 avenue du Président Wilson, 94235 Cachan cedex, France

<sup>§</sup> LPICM, UMR CNRS 7647, Ecole Polytechnique, 91128 Palaiseau, France, France

<sup>§</sup> LICSEN, CEA Saclay IRAMIS/NIMBE, 91191 Gif Sur Yvette, France

**KEYWORDS.** Phosphorescent Blue OLED, Host Material, Pure Hydrocarbons, Spirobifluorene, 4-Phenyl-spirobifluorene, Ir(ppy)<sub>3</sub>, FIrpic.

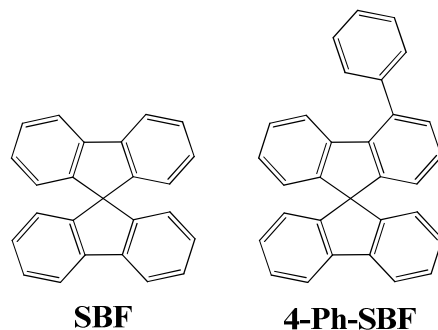
**ABSTRACT:** We report herein a new pure hydrocarbon material, 4-phenyl-9,9'-spirobifluorene (**4-Ph-SBF**), with high triplet energy level ( $E_T$ : 2.77 eV) as host for blue phosphorescent Organic Light-Emitting Diodes (PhOLEDs). Structural, thermal, electrochemical and photophysical properties have been investigated in detail and compared to its constituting building block 9,9'-spirobifluorene (**SBF**) in order to precisely study the influence of the incorporation of a phenyl unit in C4. A surprising out of plane deformation of the fluorene ring and a highly twisted structure has been notably stressed for **4-Ph-SBF** due to the substitution in C4. As both **4-Ph-SBF** and **SBF** possess a high triplet energy level (2.77/2.87 eV *resp.*), they have been successfully used as host materials for green and blue PhOLEDs. Performance of blue PhOLEDs, ca 20 cd/A, appears to be among the highest reported for pure hydrocarbon derivatives.



## INTRODUCTION

Organic light-emitting diodes (OLEDs) have attracted tremendous interest in recent years because of their potential applications in organic flat-panel displays and solid-state lighting.<sup>1-4</sup> Since organic materials are characterized by weak spin-orbit couplings, triplet excitons, generated along with singlet excitons, are lost in non radiative processes and set the maximum achievable emission quantum yield of OLED based on fluorescent materials to statistical limit of 25%. Moreover, it is difficult to develop blue-emitting materials with high efficiency, color purity and long operation times due to their intrinsically wide energy gap. As a result, the electroluminescence (EL) performance of blue OLEDs is far to be as good as that of their green- and red-EL counterparts. Among the significant progresses recently made, phosphorescent OLEDs (PhOLEDs) which use heavy-metal complexes dispersed into a host material (host/guest technique) as emitter to harvest both singlet and triplet excitons are considered as the most promising technology because, theoretically the internal quantum efficiencies of these devices may reach 100%.<sup>5-7</sup> As it is known that the primary requirement for efficient host material is that the triplet energy level ( $E_T$ ) of host should be higher than that of guest to prevent reverse energy transfer from the guest back to host and confine triplet excitons on guest molecules, the chemical design of efficient organic host materials is of great importance. In this context, the fabrication of blue PhOLEDs is still highly challenging because the prerequisites for designing organic host materials are (i) a high  $E_T$  (ii) a high glass-transition temperature ( $T_g$ ) and decomposition temperature ( $T_d$ ) and (iii) matching HOMO/LUMO levels for hole and electron injection/transport. Combining these three properties in a single molecule is far to be an easy task and to date most of host materials for blue PhOLEDs are based on carbazole, arylsilanes, phosphine oxide and triphenylamines.<sup>8-10</sup> However, despite their fantastic development as fluorescent emitters,<sup>11-14</sup> pure hydrocarbons as host materials for blue dopants are still very rare nowadays owing to the difficulty to achieve high  $E_T$ , keeping intact the other properties (thermal/morphological properties, mobility of charge carriers, HOMO/LUMO levels).<sup>6</sup> Thus, literature only reports two examples of pure hydrocarbon derivatives for blue PhOLED applications, based either on difluorenylbenzene<sup>9</sup> or on 9,9'-spirobifluorene trimer.<sup>15</sup> *Ortho* linked spirobifluorenes have recently been introduced in literature appearing as promising molecular platform.<sup>15-20</sup> However, *ortho* linked spirobifluorenes are far to be as developed as their *para* isomers, which have been widely developed in literature leading to fantastic breakthroughs in the field.<sup>21</sup> In our quest for robust pure hydrocarbon derivatives with high  $E_T$ ,<sup>22</sup> we report herein a new pure hydrocarbon host material, that is 4-phenyl-9,9'-spirobifluorene (**4-Ph-SBF**) which is a dissymmetric spirobifluorene composed of one fluorene connected through a spirocarbon to a 4-phenyl-substituted fluorene. In this work, we indeed evidenced that the C4 substitution in **4-Ph-SBF** retains the electronic properties, except the fluorescence properties, of its constituting building block 9,9'-spirobifluorene (**SBF**), while improving the thermal stabilities. Both **SBF** and **4-Ph-SBF** have been successfully used as host materials in green and blue phosphorescent OLEDs with performance of blue PhOLEDs, ca 20 cd/A, among the highest reported for pure hydrocarbon derivatives.

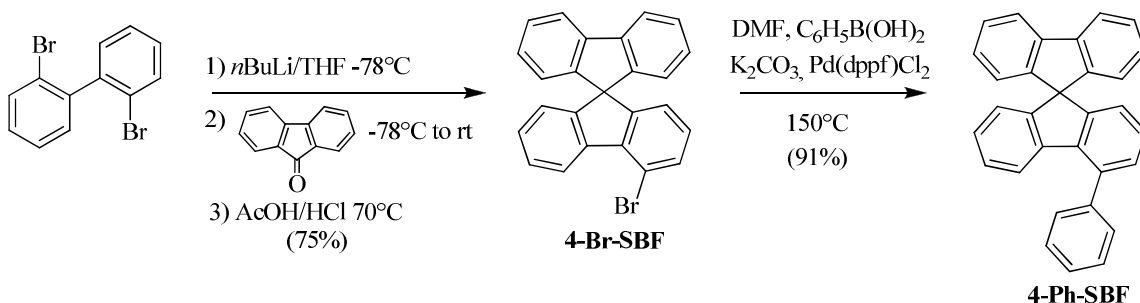
## Scheme 1: Molecules investigated in this work.



## RESULTS and DISCUSSION

The first step towards the synthesis of **4-Ph-SBF** was the obtainment of the key platform 4-bromo-9,9'-spirobifluorene (**4-Br-SBF**)<sup>16</sup> with the bromine atom already in place on the fluorenyl unit as the direct electrophilic bromination of **SBF** does not occur on the C4 position but on the C2 position.<sup>21, 23</sup> **4-Br-SBF** was hence synthesized by the mono lithium-halogen exchange of 2,2'-dibromobiphenyl followed by the trapping of the corresponding lithiated intermediate with 9-fluorenone.<sup>16</sup> The intramolecular electrophilic ring closure of the corresponding fluorenyl (not isolated), in acidic media (AcOH/HCl), further provides **4-Br-SBF** with 75 % yield (2 steps). Finally, a subsequent Suzuki cross-coupling between **4-Br-SBF** and phenylboronic acid was performed (K<sub>2</sub>CO<sub>3</sub>/Pd(dppf)Cl<sub>2</sub>) providing **4-Ph-SBF** with a high yield (91%). This synthetic approach appears to be straightforward and allows to easily obtain **4-Ph-SBF** at the multigram scale.

## Scheme 2: Synthesis of 4-Ph-SBF.



Molecular structure of **4-Ph-SBF** was further confirmed by X-ray crystallography (Figure 1). The X-ray diffraction data of single crystals of **4-Ph-SBF** reveal an asymmetric unit containing two independent molecules 1 and 2 (Figure 1).

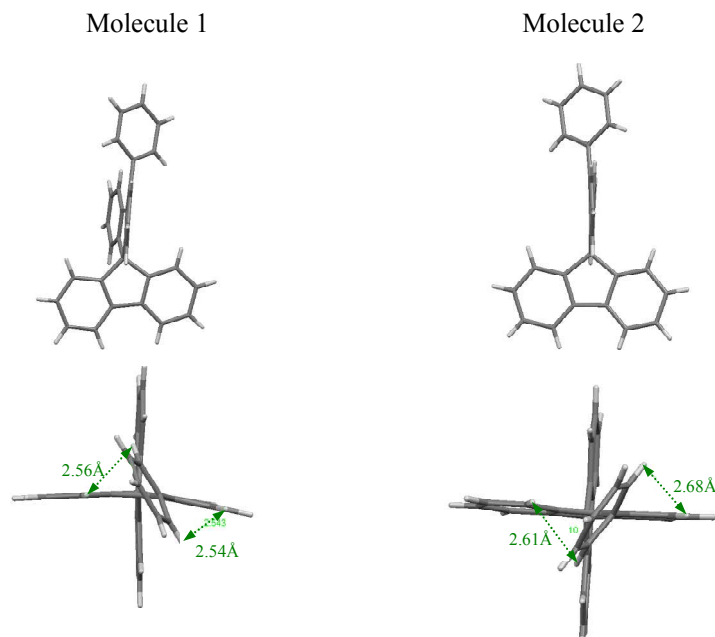


Figure 1. Molecular structure of the two molecules (left: molecule 1, right molecule 2) contained in **4-Ph-SBF** single crystal asymmetric unit.

Two important features and their consequences on the following properties need to be stressed out: (i) the relative position of the pendant phenyl ring and (ii) the deformation of the fluorenyl unit in molecule 1. Indeed, the angle between the mean plane of the pendant phenyl ring and that of its attached phenyl ring of the fluorene is of  $51.2^\circ$  in molecule 1 and  $56.6^\circ$  in molecule 2 (see SI). It is important to mention that these angles appear to be impressively larger than those reported for 2-substituted SBF (ca  $30^\circ$ ).<sup>24, 25</sup> This feature may be assigned to the steric interaction between the hydrogen atoms in *ortho* position of the pendant phenyl ring and those of the fluorenyl core (Figure 1, down). We also note that the pendant phenyl ring adopts two different conformations in molecule 1 and molecule 2 (Figure 1, bottom). In addition, we note that the distance between the hydrogen atoms in *ortho* position of the pendant phenyl ring and the two closest hydrogen atoms of the fluorenyl unit is recorded at 2.56 and 2.54 Å for molecule 1 and 2.61 and 2.68 Å for molecule 2. Thus, in the case of molecule 1, we note that the H/H distances of 2.56 and 2.54 Å are very close of the sum of their Van der Waals radii (2.4 Å).<sup>26</sup> The second feature we wish to stress in the molecular structure of **4-Ph-SBF** is the surprising deformation of the substituted fluorenyl core observed in molecule 1. Indeed, we note an angle between the phenyl units of the fluorenyl core as high as  $12.7^\circ$  in molecule 1 ( $4.8^\circ$  in molecule 2), see figure 1 and SI. This deformation in molecule 1 may be related to intermolecular packing (leading to the short H/H distances highlighted above), which can induce a folding of the fluorenyl core. These structural features are the consequence of the substitution in *ortho* position of the phenyl linkage of the fluorenyl unit (C4) and lead to a strongly more twisted structure compared to the substitution in *para* position (C2). This very unusual feature may lead to a restricted  $\pi$ -conjugation for a 4-substituted SBF compared to its 2-substituted isomer and will have remarkable consequences on the electronic properties (see below). In addition, the angle between the mean planes of the two central cyclopentadienyl units of spiro-conjugated fluorenyl cores is of  $89.8^\circ$  in molecule 1 and  $89.7^\circ$  in molecule 2, similar to that recorded in **SBF** X-Ray structure ( $89.03^\circ$ )<sup>27</sup> meaning that no deformation in the spiro-configuration is induced by the presence of the phenyl ring in C4. Finally, some short intermolecular distances are revealed, mainly CH distances but also one short C-C distance (See SI).

Geometry optimization of **SBF** and **4-Ph-SBF** in the singlet and triplet states was made with the Density Functional Theory (DFT) method based on the B3LYP hybrid functional and the 6-311+G(d,p) basis set. First, it should be mentioned that the deformation of the substituted fluorenyl core in **4-Ph-SBF** observed in the X-ray data structure (see above) is not observed in the present modelisation. In addition, the angle between the mean plane of the pendant phenyl ring and that of its attached fluorene phenyl ring has been calculated at  $70.4^\circ$  (ca  $56.6$  and  $51.2^\circ$  in the crystal, see above) meaning that the modelisation does not perfectly reflect the twist observed in the solid state and even accentuated it.

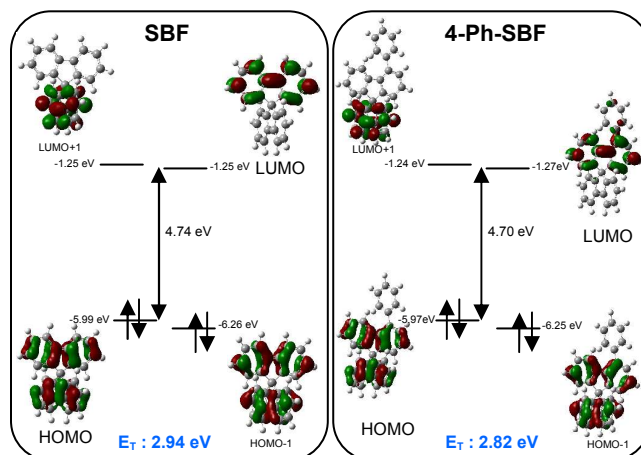


Figure 2. Calculated frontier molecular orbitals by DFT of **SBF** (left) and **4-Ph-SBF** (right), after geometry optimization at the B3LYP/6-311G+(d,p) level, shown with an isovalue of 0.04.

The calculated energy of the frontier molecular orbitals HOMO and LUMO are  $-5.99$  and  $-1.25$  eV respectively ( $\Delta E_{\text{Theo}} = 4.74$  eV) for **SBF** and  $-5.97$  and  $-1.27$  eV ( $\Delta E_{\text{Theo}} = 4.70$  eV) for **4-Ph-SBF** (figure 2). The computed triplet adiabatic  $S_0$  to  $T_1$  excitation energies, defined as the energy difference between total energy of the molecule in their respective singlet and triplet states, is of  $2.94$  eV for **SBF** and  $2.82$  eV for **4-Ph-SBF**. Furthermore, we note for both molecules that the HOMO-1/HOMO has a spirofluorenyl character whereas the LUMO/LUMO+1 exclusively has monofluorenyl character with only a very weak contribution of the phenyl in the **4-Ph-SBF** LUMO. These theoretical calculations show the similarity of **SBF** and **4-Ph-SBF** in their ground states.

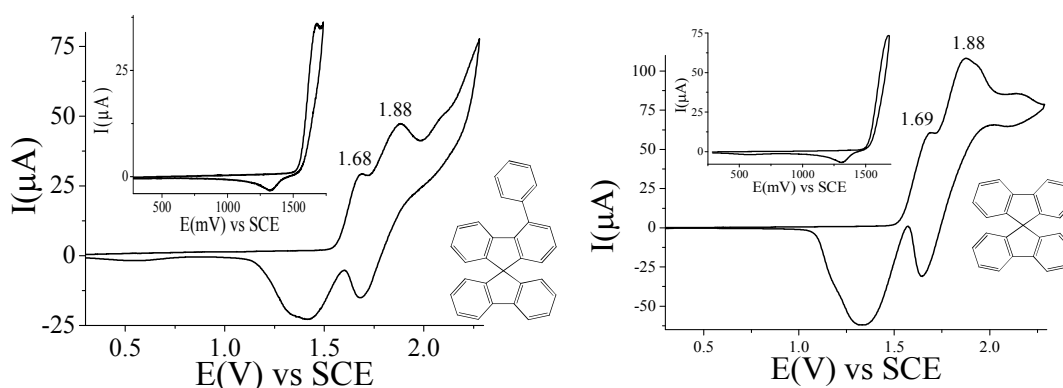


Figure 3. Cyclic voltammetry at  $100$   $\text{mV s}^{-1}$  in  $\text{CH}_2\text{Cl}_2/[\text{NBu}_4][\text{PF}_6]$   $0.2$  M in presence of **4-Ph-SBF** ( $5.2 \times 10^{-3}$  M) (left) or of **SBF** ( $10^{-2}$  M) (right). Insets zoom of the first oxidation wave. A platinum disk is used as working electrode (diameter  $1$  mm).

**4-Ph-SBF** and **SBF** present two oxidation waves in cyclic voltametry, with two maxima around 1.68/1.69 V and 1.88 V followed by less defined oxidation waves at higher potential (Figure 3). For both compounds, the first oxidation wave is irreversible (see insets) and recurrent sweeps including the two first waves lead to the apparition and the growth of new redox waves and the coverage of the electrode by an insoluble conducting polymer (see SI) as often seen for fluorene,<sup>28-31</sup> spirobifluorene<sup>31-33</sup> or dihydroindenofluorene derivatives.<sup>34</sup>

Polymers obtained from **SBF** or **4-Ph-SBF** present similar electrochemical behaviour (see SI). Although fluorene and spirobifluorene based polymers have been widely developed in litterature, the present **4-Ph-SBF** polymer seems to be the unique example of a 4-substituted spirobifluorene. This clearly shows that the substitution in C4 does not hinder the electropolymerization process and may lead to a new generation of spirobifluorenyl polymers generated by anodic oxidation.

From the onset oxidation potentials (figure 3),<sup>35</sup> we determined the HOMO level of **4-Ph-SBF** lying at -5.95 eV, identical to that of **SBF** (HOMO: -5.94 eV), indicating that the substitution in *ortho* position leads to a clear  $\pi$ -conjugation interruption. As previously stated, theoretical calculations reveal that the HOMO of both **4-Ph-SBF** and **SBF** possess a spirobifluorenyl character with both fluorene involved (See figure 2). Thus, the HOMO of **4-Ph-SBF** does not possess any electronic density on its pendant phenyl unit, confirming the  $\pi$ -conjugation interruption. This  $\pi$ -conjugation breaking may find its origin in the large angle ( $>50^\circ$ , see above) observed between the pendant phenyl ring and the fluorenyl core of **4-Ph-SBF**, leading to a highly twisted structure. It is nevertheless reasonable to content that the  $\pi$ -conjugation breaking is not total in solution and we believe that a certain degree of  $\pi$ -conjugation between the phenyl ring and the fluorene moiety occurs (see optical studies presented below). LUMO levels were determined from their onset reduction potentials<sup>35</sup> at -1.95 eV (**4-Ph-SBF**) and -1.89 eV (**SBF**), see CVs in the cathodic range in SI. Again, these values are very close and hence in accordance with the theoretical calculation conclusions presented above although the nature of the LUMOs of **4-Ph-SBF** and **SBF** are slightly different (see figure 2). The corresponding HOMO/LUMO gap ( $\Delta E_{EC}$ ) is then very large, that is 4 eV for **4-Ph-SBF** and 4.05 eV for **SBF**. The decrease of 0.05 eV between the two values appears in accordance with the small decrease (0.04 eV) found between the two calculated energy gaps (see figure 2).

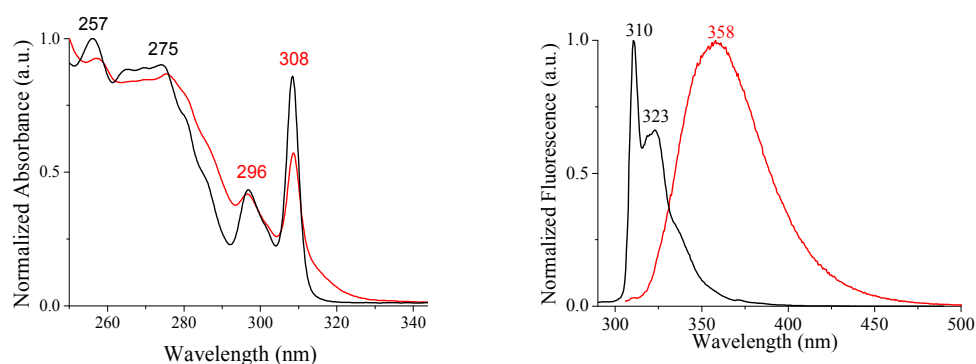


Figure 4. Absorption (left) and Emission (right) spectra of **4-Ph-SBF** (Red line,  $\lambda_{exc}$  = 309 nm) and **SBF** (Black line,  $\lambda_{exc}$  = 250 nm) in cyclohexane,  $C=10^{-6}$  M.

The UV-Vis absorption spectrum of **4-Ph-SBF** exhibits four absorption bands (257, 275, 296 and 308 nm), similar to those observed for **SBF** (figure 4, left) and for other 4-substituted oligo-SBF reported by Ma and coworkers.<sup>15, 16</sup> The main absorption band observed at 308 nm has been attributed to  $\pi$ - $\pi^*$  transition of the fluorenyl unit in **SBF** and oligo-SBF.<sup>15, 16</sup> Simulated absorption spectra obtained by TD-DFT confirm the similarity between **4-Ph-SBF** and **SBF** electronic properties in their fundamental state

(see SI). Through these calculations, the band at lower energy was assigned to HOMO/LUMO and HOMO/LUMO+1 transitions, followed however at slightly higher energy by HOMO-1/LUMO and HOMO-1/LUMO +1 more intense transitions.

For **4-Ph-SBF**, the contribution at 308 nm presents a longer wavelength tail leading to an optical energy gap ( $\Delta E_{\text{opt}}$ ) determined from the onset of the absorption spectrum (in cyclohexane) of 3.82 eV slightly more contracted (0.15 eV) than that of **SBF** (3.97 eV). The absorption tail of **4-Ph-SBF** may be due to the structural flexibility induced by the presence of the phenyl ring which may lead, for instance, to a minor proportion of conformers of the molecule with a more planar structure, allowing a certain degree of  $\pi$ -conjugation between the phenyl ring and the fluorene moiety. Interestingly, such a gap contraction is not observed for highly twisted oligo-SBFs which possess a  $\Delta E_{\text{opt}}$  of 3.93 eV independent of the number of SBF units<sup>15, 16</sup> being hence almost identical to that measured in this work for **SBF** (3.97 eV). We believe that this feature finds its origin in the impressive angle of 88.3° recorded, in the solid state, between the substituent in C4 and the fluorenyl core for the SBF dimer which lead to a complete  $\pi$ -conjugation interruption.<sup>16</sup> In these oligo-SBFs, the presence in solution of more conjugated conformers is hence surely unlikely. This result seems to confirm that in **4-Ph-SBF** a certain degree of  $\pi$ -conjugation occurs between the phenyl ring and the fluorene moiety. Thus, the bulkiness induced by the presence of the substituent in C4 and hence the angle formed between this substituent and the fluorenyl unit has a marked effect on the electronic properties of 4-substituted SBFs.

Despite very similar properties in the fundamental state, **4-Ph-SBF** and **SBF** display remarkable differences in their excited states (figure 4, right). Indeed, **4-Ph-SBF** exhibits a structureless emission spectrum ( $\lambda_{\text{max}} = 358$  nm), noticeably different in shape and wavelength compared to that of **SBF**, which presents a well-resolved spectrum ( $\lambda_{\text{max}} = 310/323$  nm) mirror image of its absorption. The quantum yields of both molecules appear nevertheless almost identical (ca 0.4). The well-resolved emission of **SBF** is similar in shape and wavelength to that of fluorene<sup>36</sup> whereas the unresolved emission of **4-Ph-SBF** appears to be like that of 4-substituted-oligo-SBF<sup>15, 16</sup> despite presenting a blue shift of ca 15 nm. This surprising loss of resolution is also observed for the rare examples of 4-substituted SBF derivatives found in literature, ie 4-diphenylphosphine oxide-SBF ( $\lambda_{\text{max}}: 346$  nm)<sup>17</sup>, 4-dibenzofuran-SBF ( $\lambda_{\text{max}}: 369$  nm)<sup>19</sup> and 4-dibenzothiophene-SBF ( $\lambda_{\text{max}}: 355$  nm).<sup>20</sup> This feature appears hence to be a unique characteristic of 4-substituted SBF derivatives as 2-substituted SBF analogues always present well resolved emission bands assigned to the double bond character of the C-C bond linking the pendant substituent and the fluorenyl core in the excited state.<sup>37, 38</sup> In addition, there is also an intriguing red shift systematically observed between 4-substituted-SBF and 2-substituted-SBF derivatives. For example, **2-Ph-SBF** and 2-dibenzofuran-SBF<sup>19</sup> present well resolved emission spectra, with maxima at 334/350 nm and 350/366 nm respectively, both being blue shifted compared to their 4-substituted analogues. If it is clear that the position of the substitution (C2 vs C4) is at the origin of this spectacular effect, more detailed theoretical and spectroscopic investigations need to be conducted to fully unravel this critical issue. The emission decay curves were recorded in cyclohexane. The lifetimes of **SBF** and **4-Ph-SBF** were measured to be 4.6 ns and 4.2 ns, respectively (see SI). Interestingly, since the lifetimes and fluorescence quantum yields are found to be very close for both compounds, we can deduce that the radiative and non-radiative rate constants are also rather similar:  $k_r(\text{SBF}) = 8.7 \times 10^7 \text{ s}^{-1}$ ;  $k_r(\text{4-Ph-SBF}) = 9.5 \times 10^7 \text{ s}^{-1}$ ;  $k_{\text{nr}}(\text{SBF}) = 1.3 \times 10^8 \text{ s}^{-1}$ ;  $k_{\text{nr}}(\text{4-Ph-SBF}) = 1.4 \times 10^8 \text{ s}^{-1}$ . Actually, it is worth noting that, despite the presence of an additional phenyl ring in the chemical structure of **4-Ph-SBF** compared to **SBF**, which in principle would allow additional non-radiative pathways of the excited state deactivation processes, the non-radiative rate constant remains almost unchanged. Consequently, we may suggest that the **4-Ph-SBF** could undergo a substantial rigidification in the excited state, such as a planarization of the structure, with the phenyl substituent conjugated to the spirofluorene core. This

hypothesis would be quite consistent with the emission red-shift and the higher Stokes shift observed for **4-Ph-SBF**, compared to **SBF**.

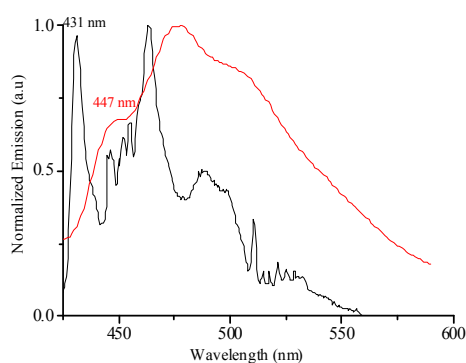


Figure 5. Emission spectra at 77 K (400/600 nm portion) in a methylcyclohexane/2-methylpentane mixture (1:1) of **4-Ph-SBF** (red line,  $\lambda_{exc}$  = 300 nm), and **SBF** (black line,  $\lambda_{exc}$  = 250 nm).

The emission spectra of **4-Ph-SBF** and **SBF** recorded at 77K follow the same trend than that observed at room temperature, with a very well resolved phosphorescence contribution for **SBF** and a non resolved phosphorescence one for **4-Ph-SBF** leading to  $E_T$  values (obtained by the highest-energy phosphorescent peak at 431 and 447 nm respectively) estimated at 2.77 eV for **4-Ph-SBF** and at 2.87 eV for **SBF**, Figure 5. These values agree quite well with theoretical calculations (2.94 eV for **SBF** and 2.82 eV for **4-Ph-SBF**, see figure 2). We however note that the  $E_T$  of **SBF** is higher than that measured by Liu and coworkers (2.7 eV).<sup>9</sup> In addition, it should be mentioned that fluorene possesses a  $E_T$  of 2.92 eV (See SI) very close to that recorded for **SBF**, meaning that the  $E_T$  in the latter is imposed the fluorenyl unit. Consequently, these results forecast that the  $E_T$  of both materials are high enough for efficient energy transfer to green emitting Ir(ppy)<sub>3</sub> ( $E_T$ : 2.42 eV) and to blue emitting FIrpic ( $E_T$ : 2.64 eV).<sup>1</sup>

**Table 1. Electronic properties of 4-Ph-SBF and SBF**

	$\lambda_{abs}^a$ (nm)	$\lambda_{PL}^a$ (nm)	$E_T^b$ (eV)	HOMO <sup>c</sup> EC/Theo	LUMO <sup>c</sup> EC/Theo	$\Delta E_{EC}/\Delta E_{opt}^d$ (eV)
4-Ph-SBF	257,275, 296,308	358	2.77	-5.95/-5.97	-1.95/-1.25	4.00/3.82
SBF	257,275, 296,308	310,323	2.87	-5.94/-5.99	-1.89/-1.27	4.05/3.97

<sup>a</sup>: Absorption and emission maxima measured in cyclohexane solution at room temperature. <sup>b</sup>: measured at 77K in methylcyclohexane/2-methylpentane mixture (1:1), <sup>c</sup>: HOMO or LUMO determined from cyclic voltametry (EC) or theoretically calculated (Theo), <sup>d</sup>:  $\Delta E_{EC}$  calculated from the HOMO and LUMO level determined through cyclic voltametry recorded in CH<sub>2</sub>Cl<sub>2</sub>;  $\Delta E_{opt}$  calculated from the onset of the absorption spectrum recorded in cyclohexane

The thermal properties of **SBF** and **4-Ph-SBF** were investigated by thermogravimetric analysis (TGA) (see SI) and differential scanning calorimetry (DSC). **SBF** and **4-Ph-SBF** are highly stable with  $T_d$ , corresponding to 5% of decomposition, recorded at 234°C and 254°C respectively. Thus, the incorporation of a pendant phenyl unit in **4-Ph-SBF** leads to an increase of  $T_d$  of ca 20°C compared to that of **SBF** highlighting hence the efficiency of the present chemical design based on a 4-substituted spirobifluorenyl scaffold.

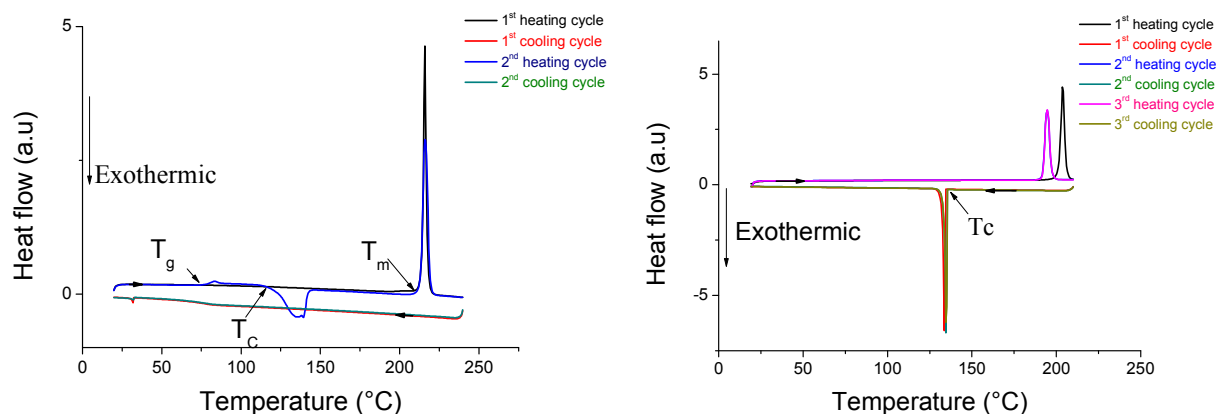


Figure 6. DSC curves of **4-Ph-SBF** (two cycles, top) and **SBF** (three cycles, bottom).

DSC was performed in the temperature range of 20 to 240°C for **4-Ph-SBF** and 20 to 210°C for **SBF** (figure 6). **4-Ph-SBF** presents on the first heating curve, a sharp endothermic peak at 216°C associated to the melting of **4-Ph-SBF** ( $T_m$ : 213°C from the peak onset). When the isotropic liquid was cooled down at the same rate from 240 to 20°C, no recrystallization occurs and the cooling leads then to an amorphous solid. When the amorphous glass sample was heated again in the second cycle, a glass transition phenomenon was observed at 83°C ( $T_g$ : 76°C from peak onset). On further heating above the  $T_g$ , an exothermic peak due to some crystallization was observed at 139°C ( $T_c$ : 115°C from peak onset). The sharp endothermic peak due to fusion is observed at 213°C again. This thermal behaviour is typical of organic glasses<sup>39</sup> and similar to amorphous molecular materials derived from **SBF** as 2,7-dithienyl-SBF for example.<sup>40</sup> The  $T_g$  value of **4-Ph-SBF** (76°C) is higher than the  $T_g$  of classical host materials for PhOLEDs such as CBP (62°C)<sup>41</sup> or *m*-CP (55°C).<sup>42</sup>

A solid sample of **SBF**, the thermal properties of which have surprisingly never been reported, presents in the first heating cycle an endothermic peak at 203°C associated to **SBF** melting ( $T_m$ : 199°C from the peak onset). When the isotropic liquid was cooled down at the same rate from 210 to 20°C, a sharp recrystallization was observed with  $T_c$  at 135°C. On the second and third heating runs, the endothermic peak is slightly shifted to 194°C ( $T_m$ : 189°C from the peak onset). This behavior indicates that **SBF** exists in a native crystalline form that is different from the crystalline form obtained after a heating and cooling cycle.

In order to explore the potential of the present pure hydrocarbons as hosts, green (Ir(ppy)<sub>3</sub>) and blue (FIrpic) PhOLEDs were fabricated and characterized. First it is important to mention that despite known for 80 years, **SBF** has, to the best of our knowledge, never been used as host material for PhOLED. Performance of the best green PhOLEDs using **4-Ph-SBF** and **SBF** as host for Ir(ppy)<sub>3</sub> are presented figure 7.

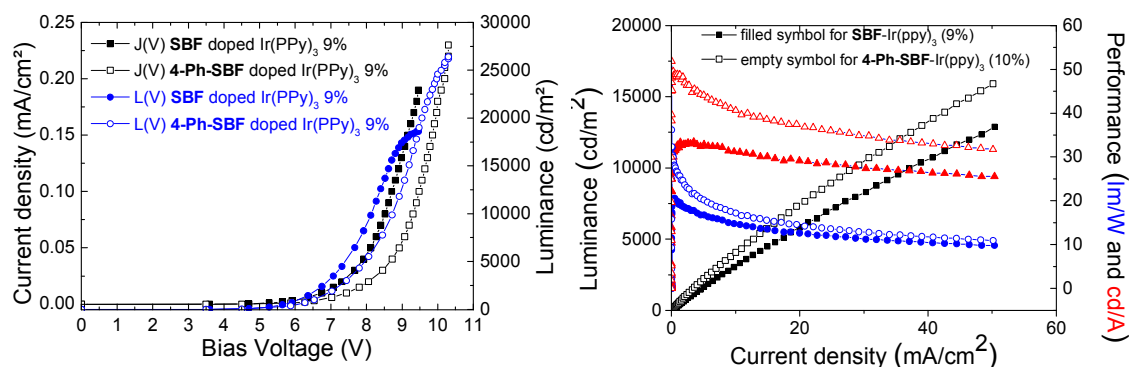


Figure 7. J-V-L characteristics (left) and Luminance, Current and Power Efficiencies versus Current Density (right) of the green devices using **4-Ph-SBF** (empty symbol) or **SBF** (filled symbol) doped with  $\text{Ir(ppy)}_3$  (9% in mass) as emitting layer.

The best performance of green PhOLEDs has been recorded with **4-Ph-SBF** as host material doped with 9% of  $\text{Ir(ppy)}_3$ . The device emits light at a low voltage of 3.5 V, with a maximum Current Efficiency (CE) of 48.1 cd/A, a maximum Power Efficiency (PE) of 36 lm/W equivalent to an External Quantum Efficient (EQE) of 10.4%. **SBF** doped with 9% of  $\text{Ir(ppy)}_3$  presents lower performance (CE=33.4 cd/A, PE= 20.5 lm/W and EQE= 8.5%) with nevertheless a slightly lower threshold voltage of 3.1 V. Both devices, reach luminance as high as 26200 and 18600  $\text{cd/m}^2$  for **4-Ph-SBF** and **SBF** based devices respectively.

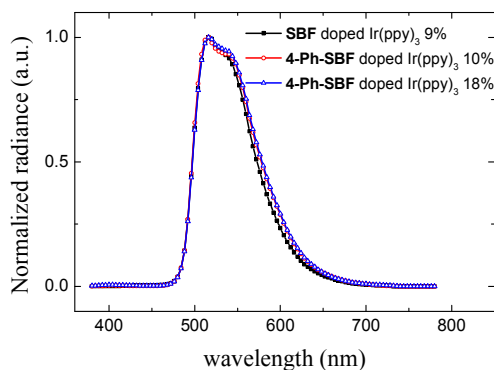


Figure 8. EL spectra of the devices: ITO/CuPc(10 nm)/NPB (40 nm)/TCTA (10 nm)/ **4-Ph-SBF** or **SBF**: $\text{Ir(ppy)}_3$  (x%) (20 nm)/TPBi (40 nm)/LiF (1.2 nm)/Al (100 nm). % dopant: 9% in **SBF** (black line); 9 or 18% in **4-Ph-SBF** (red and blue line respectively).

The EL spectra of the devices exclusively present the emission of the green dopant  $\text{Ir(ppy)}_3$  at 516/540 nm (figure 8) in accordance with the emission of pure  $\text{Ir(ppy)}_3$  film (509/540 nm).<sup>43</sup> The EL spectra are independent of the dopant ratio (9 and 18%) of the host material (Figure 8) and CIE coordinates are almost identical for both **4-Ph-SBF** (0.31 ; 0.62) and **SBF** (0.32;0.62) based PhOLEDs. With CE of ca 48 cd/A, green devices using **4-Ph-SBF** as host for  $\text{Ir(ppy)}_3$  appear to be comparable to those obtained with more complicated pure-hydrocarbon-based host materials (48.2 cd/A,<sup>15</sup> 66 cd/A,<sup>16</sup> and 60 cd/A<sup>44</sup>).

More importantly, characteristics of blue devices using phosphorescent emitter  $\text{FIrpic}$  are presented in figure 9. Contrary to green PhOLEDs, the best blue performance is obtained with **SBF** as host. This may be correlated to the highest  $E_T$  value measured for **SBF** (2.87 eV) compared to that measured for **4-Ph-SBF** (2.77 eV).

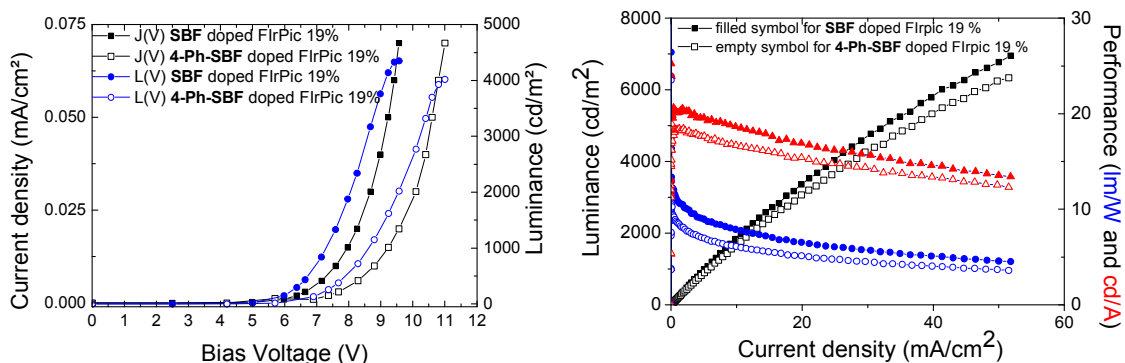


Figure 9. J-V-L characteristics (left) and Luminance, Current and Power Efficiencies versus Current Density (right) of the blue devices using **4-Ph-SBF** (empty symbol) or **SBF** (filled symbol) doped with FIrpic (19% in mass) as emitting layer.

Indeed, with a very low threshold voltage (3.3 V), blue PhOLEDs with **SBF** as host (FIrpic: 19 %) present a CE as high as 20.6 cd/A and an EQE of 6.6 %. Performance of blue PhOLEDs with **4-Ph-SBF** as host (FIrpic: 18%) reach an EQE of 5.7 %, a CE of 18.4 cd/A and a turn-on voltage of less than 4 V. Both devices, reach luminance of 4350 and 3800  $\text{cd/m}^2$  for **SBF** and **4-Ph-SBF**-based devices respectively.

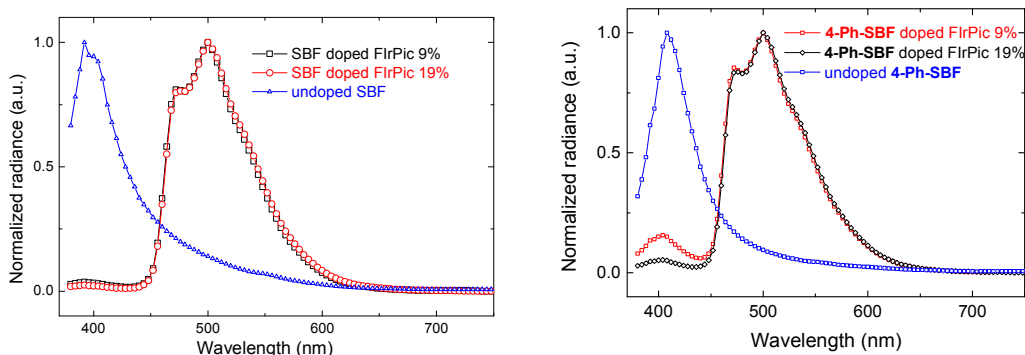


Figure 10. EL spectra (**SBF**: left, **4-Ph-SBF**: right) of the devices: ITO/CuPc(10 nm)/NPB (40 nm)/TCTA (10 nm)/ **4-Ph-SBF** or **SBF**:FIrpic (x%) (20 nm)/TPBI (40 nm)/LiF (1.2 nm)/Al (100 nm). ). % dopant: 0, 9 or 19% in **SBF**; 0, 10 or 19% in **4-Ph-SBF** (red and blue line respectively).

EL spectra of the devices presented in figure 10 reveal a main emission of the blue dopant with maxima at 473 and 500 nm in perfect accordance with the emission of pure FIrpic film (475/500 nm).<sup>45</sup> With both **4-Ph-SBF** and **SBF** as host, one observes a tiny contribution in the emission range of non-doped device (%dopant:0; blue line, figure 10). The exact origin of this band is nevertheless not clearly assigned and may arise from a recombination in the adjacent organic layers of the device. The CIEs of **SBF**- and **4-Ph-SBF**-based device are respectively calculated at (0.21 ; 0.44) and (0.19 ; 0.45).

As mentioned in the introduction, literature only reports two examples of pure hydrocarbon-based blue PhOLEDs (association of a spirobifluorene trimer with FIrpic<sup>15</sup> and association of *meta* or *para*-difluorenylbenzene with FIr6<sup>9</sup>). FIr6 is a slightly bluer dopant than FIrpic whose phosphorescence emission in solid film is centred at 460 nm.<sup>46</sup> The best CE of these devices is reported at 24.3<sup>9</sup> and 25 cd/A<sup>15</sup> with a high turn-on voltage (6.5 V) in the case of *para*-difluorenylbenzene. Compared to these blue PhOLEDs, the present devices with turn-on voltages of 3.3 to 4 V and CE of ca 20 cd/A appears therefore competitive. The present devices are also highly competitive compared to the best blue devices described with other 4-substituted-SBF as host for FIrpic such as 4-dibenzothiophene-SBF<sup>20</sup> (turn-on voltage: 6.7 V and CE : 23.5 cd/A) or 4-dibenzofuran-SBF<sup>19</sup> (turn-on voltage: 5.6 V and CE : 22.2 cd/A).

In summary, two pure hydrocarbon derivatives with high E<sub>T</sub> have been easily synthesized, at the multigram scale, through a very simple synthetic approach. In **4-Ph-SBF**, the presence of a pendant phenyl group in *ortho* position leads to twisted configuration retaining the electronic properties of its constituting building block **SBF** while improving the thermal properties. However, the fluorescence properties of these two fluorophores are noticeably different highlighting, in the excited state, the remarkable effect of substitution in *ortho* position of **SBF**. Further works, currently investigated in our groups, will concern the understanding of the drastically different fluorescence properties of 2 vs 4-substituted SBFs. Finally, green and blue PhOLEDs using **4-Ph-SBF** and **SBF** as host materials have been successfully prepared and characterized. Performance of blue PhOLEDs, ca 20 cd/A, are among the highest reported for pure hydrocarbon derivatives. This work is, to the best of our knowledge, only the third example of pure hydrocarbons as host for blue PhOLEDs and may open new avenues in the design of host materials based on pure hydrocarbon derivatives.

## EXPERIMENTAL SECTION

All manipulations of oxygen- and moisture-sensitive materials were conducted with a standard Schlenk technique. Commercially available reagents and solvents were used without further purification other than those detailed below. THF was distilled from sodium/benzophenone prior to use. Light petroleum refers to the fraction of boiling point range 40-60°C. 2.5 M solutions of n-BuLi in hexanes or THF were purchased from Sigma Aldrich. Standard 1 N solution of sulfuric acid was purchased from Alfa Aesar. 2,2'-dibromobiphenyl was purchased from Fluorochem. Reactions were stirred magnetically, unless otherwise indicated. Analytical thin layer chromatography was carried out using aluminum backed plates coated with Merck Kieselgel 60 GF254 and visualized under UV light (at 254 and 365 nm). Chromatography was carried out using Teledyne Isco CombiFlash® Rf 400 (UV detection 200-360 nm), over standard silica cartridges (Redisep® Isco). <sup>1</sup>H and <sup>13</sup>C NMR spectra were recorded using Bruker 300 MHz instruments (<sup>1</sup>H frequency, corresponding <sup>13</sup>C frequency: 75 MHz); chemical shifts were recorded in ppm and J values in Hz. In the <sup>13</sup>C NMR spectra, signals corresponding to C, CH, CH<sub>2</sub> or Me groups, assigned from DEPT, are noted. The residual signals for the NMR solvents are: CDCl<sub>3</sub>; 7.26 ppm for the proton and 77.00 ppm for the carbon, CD<sub>2</sub>Cl<sub>2</sub>; 5.32 ppm for the proton and 53.80 ppm for the carbon. The following abbreviations have been used for the NMR assignment: s for singlet, d for doublet, t for triplet and m for multiplet. High resolution mass spectra were recorded at the Centre Régional de Mesures Physiques de l'Ouest (Rennes) on (i) Bruker MicrO-Tof-Q II (Source Atmospheric Pressure Chemical Ionization (APCI-Directr introduction) (ASAP-Atmospheric Solids Analysis Probe) at a temperature of 30°C - positive mode) or on (ii) Waters Q-Tof II.

**Synthesis.** 9,9'-Spirobi[fluorene] (**SBF**) was synthesized according to published procedures,<sup>47</sup> with spectroscopic analyses and purity in perfect accordance with the literature.<sup>31, 48</sup>

4-phenyl-9,9'-spirobifluorene (**4-Ph-SBF**): 4-bromo-9,9'-spirobi[fluorene] (**4-Br-SBF**, see synthesis in SI) (0.772 g, 1.95 mmol, 1 eq), phenylboronic acid (0.325 g, 2.67 mmol, 1.37 eq), potassium carbonate (1.75 g, 12.62 mmol, 6.47 eq), Pd(dppf)Cl<sub>2</sub> (0.081 g, 0.1 mmol, 0.05 eq) were dissolved in dry DMF (20 mL). The mixture was warmed to 150°C and stirred overnight. After cooling to room temperature, saturated solution of ammonium chloride (50 mL) was added, and organic layer was extracted three times with dichloromethane (3 × 30 mL) and washed with brine (3 × 30 mL). The combined organic extracts were dried over magnesium sulfate, filtered, and concentrated under reduced pressure. The residue was purified by flash chromatography on silica gel (light petroleum) to afford a colorless solid (0.70 g). [column conditions: Silica cartridge (24 g); solid deposit on Celite®; λ<sub>detection</sub>: (254 nm, 280 nm); light petroleum at 20 mL/min; collected fraction: 15-22 min. Yield: 91%. m.p: 206°C; IR (ATR, cm<sup>-1</sup>): ν = 571, 615, 638, 654, 696, 731, 746, 1026, 1283, 1415, 1444, 1587, 3004, 3016, 3051; <sup>1</sup>H NMR (300 MHz, CD<sub>2</sub>Cl<sub>2</sub>): δ 7.85 (d, J = 7.8, 2H, ArH), 7.64-7.49 (m, 5H, ArH), 7.39 (td, J = 7.5, 0.9 Hz, 2H, ArH), 7.22-7.10 (m, 4H, ArH), 7.04 (m, 3H, ArH), 6.81 (d, J = 7.8 Hz, 2H, ArH), 6.71 (m, 2H, ArH); <sup>13</sup>C NMR (75 MHz, CD<sub>2</sub>Cl<sub>2</sub>): δ 150.0 (C), 149.7 (C), 149.6 (C), 142.4 (C), 142.2 (C), 141.5 (C), 139.2 (C), 138.6 (C), 130.3 (CH), 129.8 (CH), 129.1 (CH), 128.4 (CH), 128.3 (CH), 128.2 (CH), 128.0 (CH), 127.9 (CH), 127.8 (CH), 124.3 (CH), 124.2 (CH), 123.6 (CH), 123.3 (CH), 120.7 (CH), 66.2 (C spiro); HRMS calculated for C<sub>31</sub>H<sub>21</sub> 393.1643, found 393.1638 [M+H]<sup>+</sup>; elemental analysis calculated for C<sub>31</sub>H<sub>20</sub>: C, 94.86%; H, 5.14%. Found: C 94.29%; H 5.26%. λ<sub>abs</sub> [nm] (ε[10<sup>4</sup>.L.mol<sup>-1</sup>.cm<sup>-1</sup>]) = 297 (0.7), 308 (1.4).

**X Ray Diffraction.** Crystal was picked up with a cryoloop and then frozen at 150 K under a stream of dry N<sub>2</sub> on a APEX II Bruker AXS diffractometer for X-ray data collection (Mo Kα radiation, λ = 0.71073 Å). See details for **4-Ph-SBF** below.

**4-Ph-SBF.** C<sub>62</sub>H<sub>40</sub>; M = 784.94. APEXII, Bruker-AXS diffractometer, Mo-Kα radiation (λ = 0.71073 Å), T = 150(2) K; triclinic P-1 (I.T.#2), a = 9.7817(3), b = 13.8740(5), c = 16.0080(5) Å, α = 106.1120(10), β = 91.4430(10), γ = 92.9300(10) °, V = 2082.65(12) Å<sup>3</sup>. Z = 2, d = 1.252 g.cm<sup>-3</sup>, μ = 0.071 mm<sup>-1</sup>. The structure was solved by direct methods using the SIR97 program,<sup>49</sup> and then refined with full-matrix least-square methods based on F<sup>2</sup> (SHELXL-97)<sup>50</sup> with the aid of the WINGX<sup>51</sup> program. All non-hydrogen atoms were refined with anisotropic atomic displacement parameters. H atoms were finally included in their calculated positions. A final refinement on F<sup>2</sup> with 9483 unique intensities and 559 parameters converged at ωR(F<sup>2</sup>) = 0.1549 (R(F) = 0.0581) for 8364 observed reflections with I > 2σ(I).

**Spectroscopic studies.** Cyclohexane (analytical grade, VWR) was used without further purification. UV-visible spectra were recorded using a UV-Visible spectrophotometer SHIMADZU UV-1605. The energy gap was calculated from the absorption edge of the UV-vis absorption spectra in solution in cyclohexane, using the formula ΔE<sup>opt</sup> (eV) = hc/λ, λ being the absorption edge (in meter). With h = 6.6 × 10<sup>-34</sup> J.s (1eV = 1.6 × 10<sup>-19</sup> J) and c = 3.0 × 10<sup>8</sup> m.s<sup>-1</sup>, this equation may be simplified as: ΔE<sup>opt</sup> (eV) = 1237.5/λ (in nm). Triplet energy level was calculated from the maximum of the first phosphorescence emission peak, and conversion in electron volt was obtained with the previous formula. Corrected emission spectra were recorded with a PTI spectrofluorometer (PTI-814 PDS, MD 5020, LPS 220B) or on a Horiba Jobin-Yvon spectrofluorometer (Fluorolog FL3-221). Quantum yields in solution (Φ<sub>sol</sub>) were calculated relative to quinine sulfate (Φ<sub>sol</sub> = 0.546 in H<sub>2</sub>SO<sub>4</sub> 1N). Φ<sub>sol</sub> was determined according to the following equation,

$$\Phi_{\text{sol}} = \Phi_{\text{ref}} \times 100 \left( \frac{T_s \times A_r}{T_r \times A_s} \right) \times \left( \frac{n_s}{n_r} \right)^2$$

where, subscripts s and r refer respectively to the sample and reference. The integrated area of the emission peak in arbitrary units is given as T, n is the refracting index of the solvent ( $n_s = 1.426$  for cyclohexane) and A is the absorbance. 3 solutions of different concentration of the sample ( $A < 0.1$ ) and 3 solutions of the reference (quinine sulfate) were prepared. The quinine sulfate concentration was chosen so as the absorption of the reference and the substrate were the same at the excitation wavelength. 3 quantum yields were then calculated at this wavelength and the average value is reported. IR spectra were recorded on a Bruker Vertex 70 using a diamond crystal MIRacle ATR (Pike). Thin films were prepared by spin-coating 300  $\mu\text{L}$  of solution of THF (10 g/L) on a sapphire plate (10 mm  $\times$  10 mm) at 2500 rpm on a Süss MicroTech Labspin 6.

Fluorescence intensity decays were obtained by the time-correlated single-photon counting (TCSPC) method with femtosecond laser excitation using a Spectra-Physics set-up composed of a Titanium Sapphire Tsunami laser pumped by a doubled YAG laser Millennia. Light pulses at 900 nm were selected by optoacoustic crystals at a repetition rate of 4 MHz, and the third harmonics at 300 nm was obtained through non-linear crystals. Fluorescence photons were detected through a monochromator by means of a Hamamatsu MCP R3809U photomultiplier. The time-to-amplitude converter was purchased from Tennelec. The fluorescence data were analyzed by a nonlinear least-squares global method using the Globals software package developed at the Laboratory for Fluorescence Dynamics at the University of Illinois, Urbana-Champaign.

**Electrochemical studies.** Electrochemical experiments were performed under argon atmosphere using a Pt disk electrode (diameter 1 mm), the counter electrode was a vitreous carbon rod and the reference electrode was a silver wire in a 0.1M  $\text{AgNO}_3$  solution in  $\text{CH}_3\text{CN}$ . Ferrocene was added to the electrolyte solution at the end of a series of experiments. The ferrocene/ferrocenium ( $\text{Fc}/\text{Fc}^+$ ) couple served as internal standard. The three electrodes cell was connected to a PAR Model 273 potentiostat/galvanostat (PAR, EG&G, USA) monitored with the ECHEM Software. Activated  $\text{Al}_2\text{O}_3$  was added in the electrolytic solution to remove excess moisture. For a further comparison of the electrochemical and optical properties, all potentials are referred to the SCE electrode that was calibrated at  $-0.405$  V vs.  $\text{Fc}/\text{Fc}^+$  system. Following the work of Jenekhe,<sup>35</sup> we estimated the electron affinity (EA) or lowest unoccupied molecular orbital (LUMO) and the ionisation potential (IP) or highest occupied molecular orbital (HOMO) from the redox data. The LUMO level was calculated from:  $\text{LUMO (eV)} = -[\text{E}_{\text{onset}}^{\text{red}} (\text{vs SCE}) + 4.4]$  and the HOMO level from:  $\text{HOMO (eV)} = -[\text{E}_{\text{onset}}^{\text{ox}} (\text{vs SCE}) + 4.4]$ , based on an SCE energy level of 4.4 eV relative to the vacuum. The electrochemical gap was calculated from:  $\Delta\text{E}^{\text{el}} = |\text{HOMO-LUMO}|$  (in eV).

**Theoretical modeling.** Full geometry optimization with Density Functional Theory (DFT)<sup>52, 53</sup> and Time-Dependent Density Functional Theory (TD-DFT) calculations were performed with the hybrid Becke-3 parameter exchange<sup>54-56</sup> functional and the Lee-Yang-Parr non-local correlation functional<sup>57</sup> (B3LYP) implemented in the Gaussian 09 (Revision B.01) program suite<sup>58</sup> using the 6-311G+(d,p) basis set and the default convergence criterion implemented in the program. The figures were generated with GaussView 5.0. The computed triplet adiabatic  $S_0$  to  $T_1$  excitation energies were calculated from the difference between the total energy of the molecule in their respective singlet and triplet states.

**Thermal analysis.** ThermoGravimetric Analysis (TGA) was carried out by using TA SDT Q600 instrument, at the Ecole Nationale Supérieure de Chimie de Rennes. TGA curves were measured at 10°C/min from 0 to 600°C. Differential scanning calorimetry (DSC) was carried out by using NETZSCH DSC 200 F3 instrument equipped with an intracooler. DSC traces were measured at 10°C/min and 2 (**4-Ph-SBF**) or 3 (**SBF**) heating/cooling cycles were successively carried out and the glass transition  $T_g$  was determined from the 2<sup>nd</sup> heating cycle. Phase transition (melting, cristalisation and glass transitions) have been determined from the onset of the peak.

**Device fabrication and characterisation.** OLEDs based on a multilayer structure have been fabricated onto patterned ITO coated glass substrates from XinYan Tech (thickness: 100 nm and sheet resistance: less of 20  $\Omega$ /sq). The organic materials (from Aldrich and Lumtec) are deposited onto the ITO anode by sublimation under high vacuum ( $< 10^{-6}$  Torr) at a rate of 0.2 – 0.3 nm/s. The structure of the device is the following: ITO/CuPc(10 nm)/NPB (40 nm)/TCTA (10 nm)/ **4-Ph-SBF** or **SBF**:dopant (20 nm)/TPBi (40 nm)/LiF (1.2 nm)/Al (100 nm). In this device, ITO is used as the anode, CuPc (copper phthalocyanine) is the hole injecting layer, NPB (N,N'-di(1-naphtyl)-N,N'-diphenyl-[1,1'-biphenyl]-4,4'-diamine) is the hole-transporting layer, TCTA (4,4',4''-Tris(carbazol-9-yl)-triphenylamine) is the electron/exciton blocking layer, TPBi (1,3,5-Tris(1-phenyl-1H-benzimidazol-2-yl)benzene) is both the electron transporting layer and the hole blocking layer and a thin film of lithium fluoride covered with aluminum is the cathode. Ir(PPy)<sub>3</sub> and FIrpic are used as dopant for green and blue OLEDs respectively. The entire device is fabricated in the same run without breaking the vacuum. In this study, the thicknesses of the different organic layers were kept constant for all the devices. The active area of the devices defined by the overlap of the ITO anode and the metallic cathode was 0.3 cm<sup>2</sup>. The current-voltage-luminance (I-V-L) characteristics of the devices were measured with a regulated power supply (Laboratory Power Supply EA-PS 3032-10B) combined with a multimeter and a 1 cm<sup>2</sup> area silicon calibrated photodiode (Hamamatsu). The spectral emission was recorded with a SpectraScan PR650 spectrophotometer. All the measurements were performed at room temperature and at ambient atmosphere with no further encapsulation of devices.

## ASSOCIATED CONTENT

Supporting information

Additional graphs. This material is available free of charge via the internet at [Http://pubs.acs.org](http://pubs.acs.org)

## AUTHOR INFORMATION

Corresponding authors

\* E-Mail: [Cyril.Poriel@univ-rennes1.fr](mailto:Cyril.Poriel@univ-rennes1.fr)

\* E-Mail: [Joelle.Rault-Berthelot@univ-rennes1.fr](mailto:Joelle.Rault-Berthelot@univ-rennes1.fr)

Notes

The authors declare no competing financial interest.

## ACKNOWLEDGMENTS

We thank the CDIFX (Rennes) for X-Ray diffraction, the C.R.M.P.O for mass analysis (Rennes), the CINES (Montpellier) for computing time and the ANR (Project HOME-OLED n°ANR-11-BS07-020-01) for financial support and for a studentship (ST). We would like to highly thank Dr Franck Camerel (Rennes) for his help and advice in the understanding of thermal properties, Dr Frédéric Barrière and Prof. Abdou Boucekkine for help in DFT and TD-DFT calculations. Dr Eric Le Fur (Rennes) is also acknowledged for TGA measurements.

## REFERENCES

- 1 R. Mertens, *The OLED Handbook 2012*, A guide to OLED Technology.
- 2 K. Müllen, U. Scherf, *Organic Light-Emitting Devices: Synthesis, Properties and Applications*, Wiley-VCH Verlag GmbH & Co. KGaA, Weinheim, **2006**.
- 3 Y.-L. Chang, Z.-H. Lu, *J. Display Technol.* 2013, **9**, 459.
- 4 Special issue: p-Functional Materials, J.-L. Bredas, S. R. Marder, E. Reichmanis, *Chem. Mater.* 2011, **23**.
- 5 L. Xiao, Z. Chen, B. Qu, J. Luo, S. Kong, Q. Cong, J. Kido, *Adv. Mater.* 2011, **23**, 926.
- 6 Y. Tao, C. Yang, J. Qin, *Chem. Soc. Rev.* 2011, **40**, 2943.
- 7 M. A. Baldo, D. F. O'Brien, Y. You, A. Shoustikob, S. Sibley, M. E. Thompson, S. R. Forrest, *Nature* 1998, **395**, 151.
- 8 P.-I. Shih, C.-H. Chien, C.-Y. Chuang, C.-F. Shu, C.-H. Yang, J.-H. Chen, Y. Chi, *J. Mater. Chem.* 2007, **17**, 1692.
- 9 S. Ye, Y. Liu, C.-a. Di, H. Xi, W. Wu, Y. Wen, K. Lu, C. Du, Y. Liu, G. Yu, *Chem. Mater.* 2009, **21**, 1333–1342.
- 10 K. S. Yook, J. Y. L. Lee, *Adv. Mater.* 2012, **24**, 3169–3190.
- 11 A. C. Grimsdale, K. Müllen, *Macromol. Rapid Commun.* 2007, **28**, 1676.
- 12 D. Thirion, C. Poriel, J. Rault-Berthelot, F. Barrière, O. Jeannin, *Chem. -Eur. J.* 2010, **16**, 13646.
- 13 M. Romain, D. Tondelier, J.-C. Vanel, B. Geffroy, O. Jeannin, J. Rault-Berthelot, R. Métivier, C. Poriel, *Ang. Chem. Int. Ed.* 2013, **52**, 14147–14151.
- 14 N. Cocherel, C. Poriel, J. Rault-Berthelot, F. Barrière, N. Audebrand, A. M. A. Slawin, L. Vignau, *Chem. -Eur. J.* 2008, **14**, 11328.
- 15 C. Fan, Y. Chen, P. Gan, C. Yang, C. Zhong, J. Qin, D. Ma, *Org. Lett.* 2010, **12**, 5648–5651.
- 16 Z. Jiang, H. Yao, Z. Zhang, C. Yang, Z. Liu, Y. Tao, J. Qin, D. Ma, *Org. Lett.* 2009, **11**, 2607–2610.
- 17 S. E. Jang, C. W. Joo, J. S. Ok, Y. K. Soo, J. Y. Lee, *Org. Elec.* 2010, **11**, 1059.
- 18 K. H. Lee, S. O. Kim, K. S. Yook, S. O. Jeon, J. Y. Lee, S. S. Yoon, *Synt. Met.* 2011, **161**, 2024.
- 19 S.-C. Dong, C.-H. Gao, Z.-H. Zhang, Z.-Q. Jiang, S.-T. Lee, L.-S. Liao, *Phys. Chem. Chem. Phys.* 2012, **14**, 14224.
- 20 S.-C. Dong, C.-H. Gao, X.-D. Yuan, L.-S. Cui, Z.-Q. Jiang, S.-T. Lee, L.-S. Liao, *Org. Elec.* 2013, **14**, 902.
- 21 T. P. I. Saragi, T. Spehr, A. Siebert, T. Fuhrmann-Lieker, J. Salbeck, *Chem. Rev.* 2007, **107**, 1011.

- 22 C. Poriel, R. Métivier, J. Rault-Berthelot, D. Thirion, F. Barrière, O. Jeannin, *Chem. Commun.* 2011, **47**, 11703.
- 23 J. Pei, J. Ni, X.-H. Zhou, X.-Y. Cao, Y.-H. Lai, *J. Org. Chem.* 2002, **67**, 4924.
- 24 K.-T. Wong, Y.-L. Liao, Y.-C. Peng, C.-C. Wang, S.-Y. Lin, C.-H. Yang, S.-M. Tseng, G.-H. Lee, S.-M. Peng, *Cryst. Growth Des.* 2005, **5**, 667–671.
- 25 E. Demers, T. Maris, J. D. W. Wiest, *Cryst. Growth Des.* 2005, **5**, 667.
- 26 I. N. Levine, *Physical Chemistry-Fifth Edition*, MacGraw.
- 27 H. Schenk, *Acta Crystallogr., Sect. B: Struct. Crystallogr. Cryst. Chem.* 1972, **28**, 625.
- 28 J. Rault-Berthelot, J. Simonet, *New J. Chem.* 1986, **10**, 169.
- 29 J. Rault-Berthelot, L. Angely, J. Delaunay, J. Simonet, *New J. Chem.* 1987, **11**, 487.
- 30 J. Rault-Berthelot, M. M. Granger, J. Simonet, H. Le Deit, V. Le Menn-Questaigne, M. Massaudi, J. Tahri-Hassani, *J. Chim. Phys.* 1995, **92**, 867.
- 31 J. Rault-Berthelot, M.-M. Granger, L. Mattiello, *Synth. Met.* 1998, **97**, 211.
- 32 C. Poriel, Y. Ferrand, P. Le Maux, J. Rault-Berthelot, G. Simonneaux, *Inorg. Chem.* 2004, **43**, 5086.
- 33 Y. Ferrand, C. Poriel, P. Le Maux, J. Rault-Berthelot, G. Simonneaux, *Tet. Asym.* 2005, **16**, 1463.
- 34 J. Rault-Berthelot, C. Poriel, F. Justaud, F. Barrière, *New J. Chem.* 2008, **32**, 1259.
- 35 A. P. Kulkarni, C. J. Tonzola, A. Babel, S. A. Jenekhe, *Chem. Mater.* 2004, **16**, 4556–4573.
- 36 D. Horhant, J.-J. Liang, M. Virboul, C. Poriel, G. Alcaraz, J. Rault-Berthelot, *Org. Lett.* 2006, **8**, 257.
- 37 R. M. Belletête M., Beaupré S., Leclerc M., Durocher G., *Chem. Phys. Lett.* 2000, **316**, 101.
- 38 J.-F. Wang, J.-K. Feng, A.-M. Ren, L. Yang, *Chin. J. Chem.* 2005, **23**, 1618.
- 39 K. Naito, A. Miura, *J. Phys. Chem.* 1993, **97**, 6240.
- 40 J. Pei, J. Ni, X.-H. Zhou, X.-Y. Cao, Y.-H. Lai, *J. Org. Chem.* 2002, **67**, 8104.
- 41 M.-H. Tsai, Y.-H. Hong, C.-H. Chang, H.-C. Su, C.-C. Wu, A. Matoliukstyte, J. Simokaitiene, S. Grigalevicius, J. V. Grazulevicius, C.-P. Hsu, *Adv. Mater.* 2007, **19**, 862.
- 42 S.-J. Yeh, M.-F. Wu, C.-T. Chen, Y.-H. Song, Y. Chi, M.-H. Ho, S.-F. Hsu, C. H. Chen, *Adv. Mater.* 2005, **17**, 285.
- 43 J. H. Seo, N. S. Han, H. S. Shim, J. H. Kwon, J. K. Song, *Bull. Korean Chem. Soc.* 2011, **32**, 1415.
- 44 L.-C. Chi, W.-Y. Hung, H.-C. Chiu, K.-T. Wong, *Chem. Commun.* 2009, 3892.
- 45 N. S. Han, S. H. Sohn, S. M. Park, J. K. Song, *Bull. Korean Chem. Soc.* 2013, **34**, 1547.
- 46 D. A. B. W. Holmes R. J., Forrest S. R., Ren X., Li J., Thompson M. E., *Appl. Phys. Lett.* 2003, **83**, 3818.
- 47 V. Prelog, D. Bedekovic, *Helv. Chim. Acta* 1979, **62**, 2285–2302.
- 48 C. Poriel, Y. Ferrand, S. Juillard, P. Le Maux, G. Simonneaux, *Tetrahedron* 2004, **60**, 145.
- 49 A. Altomare, M. C. Burla, M. Camalli, C. Casciarano, A. Giacovazzo, A. Guagliardi, A. G. G. Moliterni, G. Polidori, R. Spagna, *J. Appl. Cryst.* 1999, **32**, 115.
- 50 G. M. Sheldrick, *Acta Crystallogr.* 2008, **A64**, 112.
- 51 L. J. Farrugia, *J. Appl. Cryst.* 2012, **45**, 845.
- 52 P. Hohenberg, W. Kohn, *Phys. Rev.* 1964, **136**, B864.
- 53 J.-L. Calais, *Int. J. Quantum Chem.* 1993, **47**, 101.
- 54 A. D. Becke, *Phys. Rev. A* 1988, **38**, 3098.
- 55 A. D. Becke, *J. Chem. Phys.* 1993, **98**, 5648–5652.
- 56 A. D. Becke, *J. Chem. Phys.* 1993, **98**, 1372.
- 57 C. Lee, W. Yang, R. G. Parr, *Phys. Rev. B* 1988, **37**, 785.
- 58 M. J. Frisch, G. W. Trucks, H. B. Schlegel, G. E. Scuseria, M. A. Robb, J. R. Cheeseman, G. Scalmani, V. Barone, B. Mennucci, G. A. Petersson, H. Nakatsuji, M. Caricato, X. Li, H. P.

Hratchian, A. F. Izmaylov, J. Bloino, G. Zheng, J. L. Sonnenberg, M. Hada, M. Ehara, K. Toyota, R. Fukuda, J. Hasegawa, M. Ishida, T. Nakajima, Y. Honda, O. Kitao, H. Nakai, T. Vreven, J. A. J. Montgomery, J. E. Peralta, F. Ogliaro, M. Bearpark, J. J. Heyd, E. Brothers, K. N. Kudin, V. N. Staroverov, T. Keith, R. Kobayashi, J. Normand, K. Raghavachari, A. Rendell, J. C. Burant, S. S. Iyengar, J. Tomasi, M. Cossi, N. Rega, J. M. Millam, M. Klene, J. E. Knox, J. B. Cross, V. Bakken, C. Adamo, J. Jaramillo, R. Gomperts, R. E. Stratmann, O. Yazyev, A. J. Austin, R. Cammi, C. Pomelli, J. W. Ochterski, R. L. Martin, K. Morokuma, V. G. Zakrzewski, G. A. Voth, P. Salvador, J. J. Dannenberg, S. Dapprich, A. D. Daniels, O. Farkas, J. B. Foresman, J. V. Ortiz, J. Cioslowski, D. J. Fox, Gaussian 09, Revision B.01, Gaussian, Inc., Wallingford CT, 2010.